ASPS Conference Proceedings 1: 1791-1802 (2022)

Proceedings of

12th Structural Engineering Convention-An International Event (SEC 2022)

Available at https://asps-journals.com/index.php/acp

Experimental Studies on Blast Performance of Unreinforced Masonry Walls: A state-of-the-art review

S.M. Anas [1, *], Mehtab Alam [2], Mohammad Umair [3]

[1] Department of Civil Engineering, Ph.D. Scholar, Jamia Millia Islamia, New Delhi, 110 025, India
[2] Department of Civil Engineering, Professor, Jamia Millia Islamia, New Delhi, 110 025, India
[3] Department of Civil Engineering, Assistant Professor, Jamia Millia Islamia, New Delhi, 110 025, India

Paper ID - 260445

Abstract

A large proportion of India's residential buildings is of unreinforced masonry (URM) and falls under the category of non-engineered structures. URM walls in the residential buildings, customarily constructed from clay bricks or concrete blocks and cut stones, are found to be braced and therefore able to carry some out-of-plane loads produced by wind and earthquake, and survive. However, they are found to be more vulnerable to high air-pressure generated by explosive-induced detonations. Sufficient amount of investigations has been made by engineers to study the effect of brick strength, mortar strength, boundary conditions, wall thickness, and Young's modulus of masonry on the blast performance of the URM walls. In this paper, available experimental studies on clay-brick and concrete block URM walls subjected to explosive-induced blast loading are briefly reviewed and summarized in tabular form. Studies conducted to improve the blast resistance of the walls using GFRP strips, GFRP rods, and Polyurea coating, and their effect on mid-span deflection, damage, and cracks have also been reviewed. It has been observed that the effect of brick strength and mortar strength on maximum mid-span deflection and damage resistance of the walls is insignificant under higher peak reflected blast pressures (> 2 MPa). Besides, the walls strengthened with the GFRP strips or Polyurea coating performed better with regards to mid-span deflection, damage, and cracking. The influence of Young's modulus of masonry on the blast response of the walls is found to be more effective in reducing the maximum mid-span deflection. Also, the failure mechanism of the walls is found to be highly dependent upon the peak overpressure, duration of the blast, and support conditions.

Keywords: Blast loading, Unreinforced masonry (URM) wall, Clay bricks, Concrete blocks, Polyurea coating, Glass fiber reinforced polymer (GFRP) grids, GFRP rods, GFRP strips, Blast parameters, Cracks, Damage, Failure modes

1. Introduction

Masonry work is one of the oldest building crafts which is still widely used in the construction of buildings [11, 27]. It has developed itself a great reputation as one of the leading traditional construction materials of the building. Inherent advantages of masonry include appeasing aesthetics, longevity, durability, heat absorber, environmental-friendly, sound isolation, fire resistance, and economic considerations, contribute to its continuing appeal [6, 7]. Moreover, masonry is reusable and recyclable and its ingredients are also locally available at affordable prices. There are various types of masonry walls used in the construction of the buildings, however, the most common of which may be classified as stone masonry such as rubble- and ashlar- masonry, burnt-clay masonry, cavity wall masonry, hollow masonry unit (CMU), reinforced hollow masonry unit, solid masonry such as concrete or clay brick units, reinforced grouted masonry unit, and grouted masonry unit [16].

Recent accidental explosions and subversive blasts have drawn attention to the vulnerability and sustainability of the buildings and infrastructure subjected to blast loadings [10]. Damage caused by the blast ranges from reparable to collapse with considerable loss of life depends on the magnitude of peak overpressure generated from the explosion and blast resistance of the structure/building. Some recent examples are the Beirut explosion (August 2020), the explosion at an ammunition warehouse in Ryazan City (October 2020), the bombing on a school building in Peshawar City (November 2020), and the bombing and attack on the Kabul University (November 2020). Numerous attacks have been directed toward embassies, and suicide car bombers have been used to target populated areas in different parts of the world [21]. In cases where structural collapse is not an issue, flying debris/splinters caused serious injuries and even loss of life of innocent civilians. Of particular concerns are unreinforced masonry (URM) infills walls. Structural systems composed of a reinforced concrete framing system with the URM infill walls make up a significant portion of the building inventory in India and around the world [10]. Being unreinforced, these walls have negligible resistance to resist lateral loads such as induced by explosions. As a result, efforts have been undertaken to

*Corresponding author. Tel: +91-8527764166; E-mail address: mohdanas43@gmail.com

Published online: December 19, 2022
doi:10.38208/acp.v1.720

investigate the effect of brick strength, mortar strength, boundary conditions, wall thickness, and Young's modulus of masonry on the blast response of the clay brick and concrete block URM walls.

2. Review of the URM walls subjected to blast loading

Significant experimental research has been conducted concerning the dynamic response of the URM walls subjected to blast-induced impulsive loadings (Carney P. and Myers J. J., 2005 [10]; Hrynyk D. T. and Myers J. J., 2008 [14]; Zapata J. B. and Weggel C. D., 2008 [26]; Wei X. and Stewart G. M., 2010 [24]; Abou-Zeid M. B. et al., 2011 [2]; Ahmad S. et al., 2014 [3]; Joao P. et al., 2014 [17]; Pereira M. J. et al., 2015 [20]). The aim of the experimental studies conducted so far has been, firstly, to study the nature of air-blast wave and its characteristics, and secondly, to conduct parametric investigations to study the effect of brick strength, mortar strength, boundary condition, wall thickness, tensile strength, and Young's modulus of masonry on the blast performance of the walls.

2.1 Carney P. and Myers J. J. (2005) [10]

The authors experimentally examined the out-of-plane response of the URM walls, strengthened with the glass fiber reinforced polymer (GFRP) strips and rods, under static and air-blast loadings (Figs.- 1&2). The static loading was applied to one face of the wall using an airbag system. Explosive charge weight of 1.80 kg pentolite was considered at varying standoff distances. The investigation was conducted in two phases namely; Phase I and Phase II (Fig.-3). Phase I consisted of two series. Series I was composed of six walls (Walls #1 - #6), while Series II consisted of additional six walls (Walls #7 - #12). The walls in Phase I were subjected to static loading. Phase II was composed of two walls subjected to blast loading. Fig.-4 shows the test setup for Phase I. Fig.-5 shows the test setup for Phase II. The walls in both phases were constructed with concrete blocks (CMUs) of size 101.60 mm x 203.20 mm x 304.80 mm. The nominal thickness of the GFRP sheet was 0.35 mm. The diameter of the GFRP rod was 6.35 mm. The tensile strength and Young's modulus of the rod were 827.37 MPa and 40.81 GPa, respectively. The ultimate tensile strength, Young's modulus, and ultimate rupture strain were 1517 MPa, 72.39 GPa, and 2.10%, respectively. Fig.-6 shows the observed crack patterns and damage in the tested walls. Fig.-7 shows the observed failure modes of walls of Phase II. Results revealed that the walls retrofitted with the GFRP sheet were performed better than the walls retrofitted with the GFRP rods and un-retrofitted walls under both static and blast loadings. The experimental pressures were compared and found to be in good agreement with the predictions of the theoretical model.

2.2 Hrynyk D. T. and Myers J. J. (2008) [14]

A series of tests were conducted to investigate the deflection performance of the URM walls, strengthened with the glass fiber reinforced polymer (GFRP) grid and Poly-urea coating, subjected to a uniform pressure applied using an airbag system as shown in Fig.-8. A total of eight URM walls were tested. Three out of the eight walls were constructed with the wood-fiber fly ash (WFFA) material, two walls were constructed with the clay bricks (CL), and three walls with the concrete blocks (CMUs). Two retrofitting schemes were adopted: (1) Polyurea coating (PU), and (2) GFRP grid with polyurea coating (PU-G). Fig.-9 shows the test matrix of the tested walls. The compressive strength of the WFFA, CL, and CMU masonry units were 6.90 MPa, 10.30 MPa, and 9.00 MPa, respectively. All the walls had a uniform width of 914.40 mm and a constant height-to-thickness ratio of 13.20. Type-S mortar (12.70 MPa) as per ASTM (2005) [5] was used for the wall construction. The tensile strength, Young's modulus, and ultimate strain of the GFRP grids were 600 MPa, 26.62 GPa, and 0.023, respectively. The tensile strength and Young's modulus of the polyurea were 6.90 MPa and 83 MPa. Three different failure modes were observed namely; instability failure, flexural failure, and anchorage failure of the polyurea. Fig.-10 shows the failure modes of the tested walls. No crushing was observed in the walls CL-0 and CMU-0. Crushing was observed at mid-height of the wall WFFA-0 due to the low compressive strength of WFFA. It was concluded that the deflection performance of the walls strengthened with a 3 mm thick layer of polyurea coating was superior to the walls retrofitted with PU-G (Fig.-11). However, the out-of-plane load capacity of the walls retrofitted with PU-G was much higher than that with the un-retrofitted walls, and that with the walls retrofitted with PU (see Fig.-11).

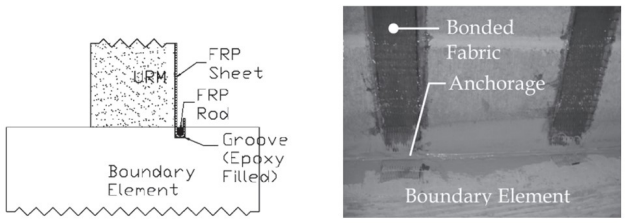

Fig. 1. GFRP laminate detail (Carney P. and Myers J. J., 2005)

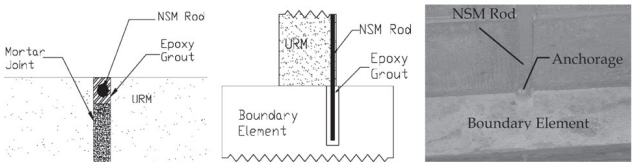

Fig. 2. GFRP rod detail (Carney P. and Myers J. J., 2005)

Walls			Retrofit Scheme					
			FRP Sheets	Sheet Width	NSM FRP Rods	Anchor-age	Stacked Bond	Running Bond
Phase I	Series I	#1					√	
		#2					√	
		#3	√	2.5"		√	√	
		#4	√	2.5"		√	√	
		#5			√	√	√	
		#6			√	√	√	
	Series II	#7	√	2.5"			√	
		#8			√		√	
		#9			√	√		√
		#10	√	2.5"		√		√
		#11	√	4.5"		√	√	
		#12	√	6.5"		√	√	
Phase II		#1	√	2.5"			√	
		#2	√	2.5"		√	√	

Conversion: 1in = 25.4 mm Key: √ - includes detail

Fig. 3. Test matrix (Carney P. and Myers J. J., 2005)

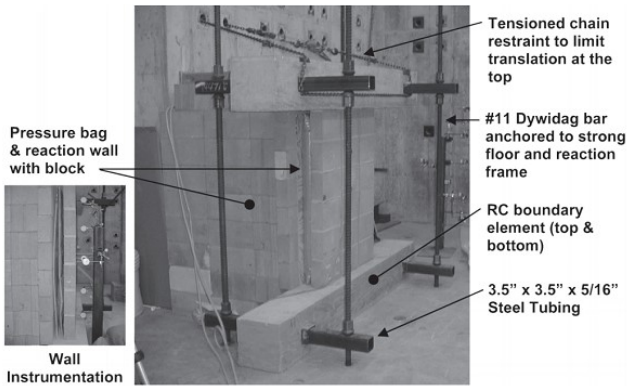

Fig. 4. Test setup for Phase I (Carney P. and Myers J. J., 2005)

Fig. 5. Test setup for Phase II (Carney P. and Myers J. J., 2005)

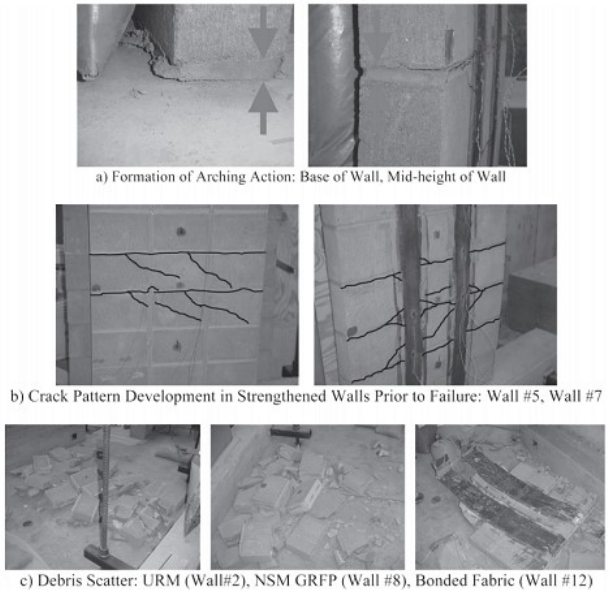

Fig. 6. Observed crack patterns and damage in the tested walls (Carney P. and Myers J. J., 2005)

Wall	Charge Weight (lb)	Standoff Distance (ft)	Level of Damage
Wall #1	2	6	Light Damage
	4	6	Failure
Wall #2	3	6	Light Damage
	4	6	Heavy Damage
	5	6	Failure

Fig. 7. Observed failure modes of walls of Phase II (Carney P. and Myers J. J., 2005)

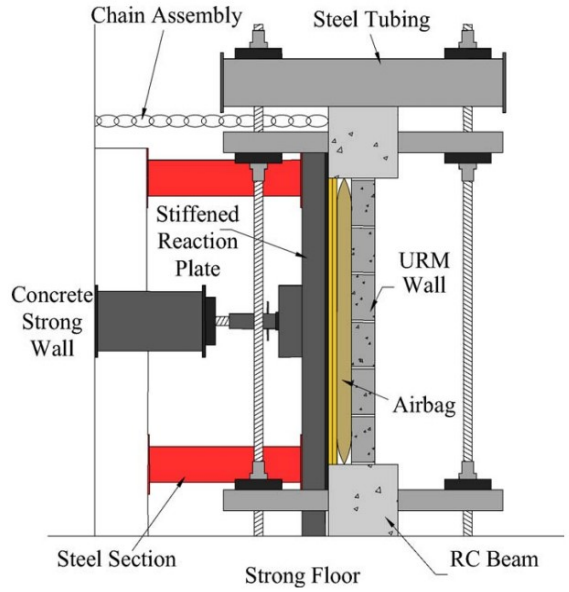

Fig. 8. Test setup (Hrynyk D. T. and Myers J. J., 2008)

Wall	Wall thickness (mm (in.))	(h/t)	$\rho_{FRP}(E_{FRP}/E_m)\times 100$	Retrofit scheme
CMU-0	92 (3.63)	13.2	—	None
CMU-PU	92 (3.63)	13.2	(Neglected)	Polyurea
CMU-PU-G	92 (3.63)	13.2	1.36	GFRP–polyurea
WFFA-0	70 (2.75)	13.1	—	None
WFFA-PU	70 (2.75)	13.1	(Neglected)	Polyurea
WFFA-PU-G	70 (2.75)	13.1	3.00	GFRP–polyurea
CL-0	70 (2.75)	13.1	—	None
CL-PU-G	70 (2.75)	13.1	2.00	GFRP–polyurea

Fig. 9. Test matrix of the walls tested by Hrynyk D. T. and Myers J. J. (2008) [14]

2.3 Zapata J. B. and Weggel C. D. (2008) [26]

The authors conducted an explosion test inside a 2-storey unreinforced brick masonry wall building scheduled to be demolished. The objectives of the study were: (1) to investigate the capabilities of various numerical methods to estimate blast pressure generated from the on-ground cylindrical-shaped explosive charge of weight 8.71 kg, and (2) to examine the blast response of the ordinary load-bearing wall building. Fig.-12 shows the façade of the building and blast chamber. The load-bearing walls were 300 mm thick and partition walls were 200 mm thick. The average compressive strength and tensile strength of the masonry were 13.10 MPa and 0.862 MPa, respectively. The diameter of the explosive charge was 170 mm and its height was approximately 410 mm. Results revealed that the three walls closest to the explosion were severely damaged. Figs. 13-15 show the observed crack patterns on each wall. The partition wall (Wall #1) experienced a maximum permanent displacement of 250 mm (at Location A). Regions of the load-bearing walls (Wall #2 and Wall #3) were found to be heavily damaged. The experimental results were compared and found to be in good agreement with those computed from the single-degree-of-freedom blast effects design

spreadsheet (SBEDS) method. Two criteria were proposed to define the state of the load-bearing wall relative to its collapse limit state. The first criterion was the displacement criterion which defines the state of the load-bearing wall as the ratio of the permanent mid-height deflection to the failure deflection. The second criterion was the resistance criterion which defines the state of the bearing wall as the ratio of the residual resistance to the maximum resistance.

2.4 Irshidat M. et al. (2009) [15]

The authors investigated the effect of polyurea coating (PU), polyurea with exfoliated graphene nanoplatelets (PU-XGnP), and polyurea with polyhedral oligomeric silsesquioxane (PU-POSS) on the blast response of the URM walls. A total of three walls were tested using the shock tube (blast wave simulator). The top and bottom edges of the target wall were restrained with the steel frame. All the walls were constructed with 115 mm x 54 mm x 57 mm concrete blocks (CMUs). The ultimate strengths of the PU, PU-XGnP, and PU-POSS were 11.85, 4.48, and 13.51 MPa, respectively. The ultimate strain of the PU, PU-XGnP, and PU-POSS were 95%, 96%, and 113%, respectively. Results revealed that Wall #2 (Wall with PU-XGnP) experienced a maximum mid-span deflection of 273.05 mm under the blast pressure of 1.254 MPa. The wall with PU-POSS (Wall #3) suffered lesser damage and mid-span deflection (120.65 mm) than the wall with PU and the wall with PU-XGnP when subjected to similar explosive loads which confirms that PU-POSS is a more effective material for blast design. Figs. 16-18 show the observed damage in the tested walls.

(a)

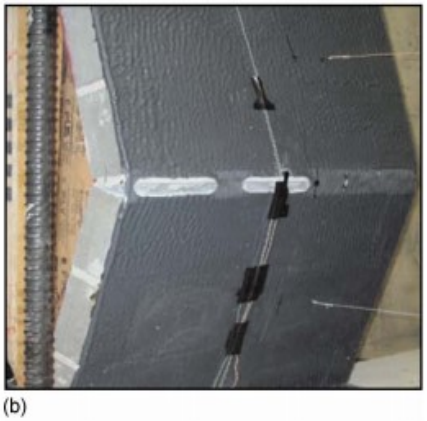

(b)

(c)

Fig. 10. Failure modes of URM walls tested by Hrynyk D. T. and Myers J. J. (2008) [14]: (a) scattering of debris in control wall, (b) failure of CMU-PU wall, and (c) collapse of wall WFFA-PU-G

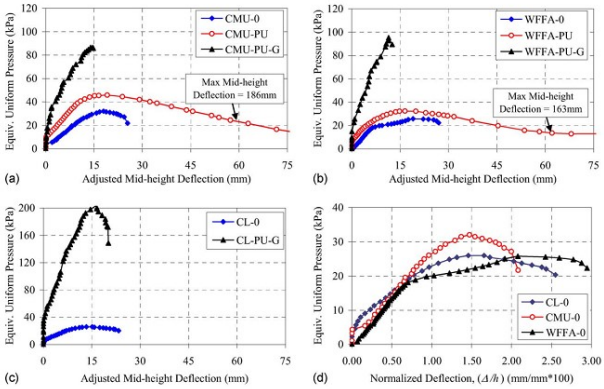

Fig. 11. Comparison of responses for different series of URM walls tested by Hrynyk D. T. and Myers J. J. (2008) [14]: (a) CMU, (b) WFFA, (c) CL, and (d) effect of masonry

2.5 Wei X. and Stewart G. M. (2010) [24]

Wei X. and Stewart G. M. (2010) conducted parametric investigations to examine the effect of mortal strength, brick strength, wall thickness, and boundary condition on the deflection performance of the URM walls, constructed with clay bricks, subjected to reflected peak pressures generated from 125 kg TNT charge detonated at standoff distances of 20, 25, and 30 m in the free field. The tests were conducted on three different walls of sizes 3590 mm x 2656 mm x 110 mm, 3590 mm x 2656 mm x 230 mm, and 3590 mm x 2656 mm x 350 mm. The dimensions of the clay bricks were 230 mm x 110 mm x 76 mm. The thickness of the mortar was 10 mm. Fig.-20 shows the mechanical properties of three types of mortar (M5, M10, and M15) and three types of clay bricks (B20, B30, and B40), where "σ_{sc0}" is quasi-static compressive strength, "σ_{st0}" is the quasi-static tensile strength, "σ_{sttt0}" is the quasi-static strength under hydro-tension, "ν" is the Poisson's ratio, "ε_{sc0}" is the quasi-static threshold compressive strain, and "ε_{st0}" is the quasi-static threshold tensile strain. The reflected peak pressures obtained from the experiment were compared and found to be in good agreement with those computed using CONWEP 2.0 model available in the LS-DYNA software. The effect of mortar strength on the performance of the walls was

investigated with three mortar strength (M5, M10, and M15), B40 brick, and with a wall thickness of 110 mm. Fig.-21 shows the deflection time-history of the walls with three mortar strength and B40 brick at different standoff distances. The arrival time of the air-blast wave at standoff distances of 20 and 30 m was estimated to be 0.03 and 0.06 sec, respectively. After the wall of size, 3590 mm x 2656 mm x 110 mm was exposed to a charge weight of 125 kg TNT at a standoff distance of 20 m, it was noticed that the difference between the maximum deflections with different mortar strength (M5 to M15) was almost negligible and the maximum deflections of the walls with B40 bricks were much larger than the wall thickness (110 mm). When the detonation distance was increased to 25 m, all maximum deflections were reported to be more than 110 mm. However, when the detonation distance was increased to 30 m, the maximum deflections of the walls were found to be lesser than the thickness of the wall (110 mm).

Furthermore, the effect of brick strength on the deflection performance of the URM walls was studied with three brick strength (B20, B30, and B40), M5 mortar, and with a wall thickness of 110 mm. Fig.-22 shows the maximum deflection time-response of 110 mm thick walls with three brick strength and M5 mortar at standoff distances of 20, 25, and 30 m. It was reported that the effect of the mortar strength and brick strength on the deflection performance of 110 mm thick walls was insignificant under higher reflected peak pressures (>2 MPa). The effect of the boundary conditions on the deflection behavior of the URM walls was investigated with wall thickness 110 mm and four typical boundary conditions, shown in Fig.-23(A). It was reported that the wall with Type-A boundary condition experienced maximum deflection, while the wall with Type-D suffered lesser deflection in comparison to other boundary conditions considered (see Fig.-23). Moreover, the effect of wall thickness on the deflection response of the walls was examined with B40 bricks, M5 mortar, Type-B boundary condition, and with three different wall thicknesses of 110, 230, and 350 mm. Fig.-23(B) shows the deflection time-history of the walls of different thicknesses considered. When they detonated 125 kg TNT charge at a standoff distance of 20m, the maximum deflection in both 110 and

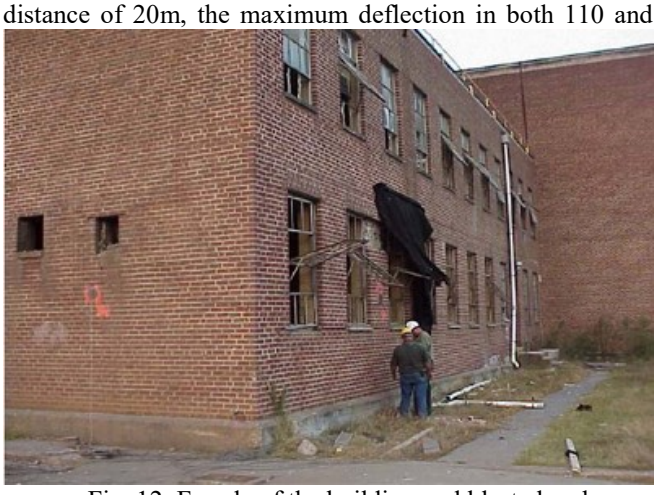

Fig. 12. Façade of the building and blast chamber showing solid Wall #2 (on the left) and Wall #3 with windows on the right (Zapata J. B. and Weggel C. D., 2008)

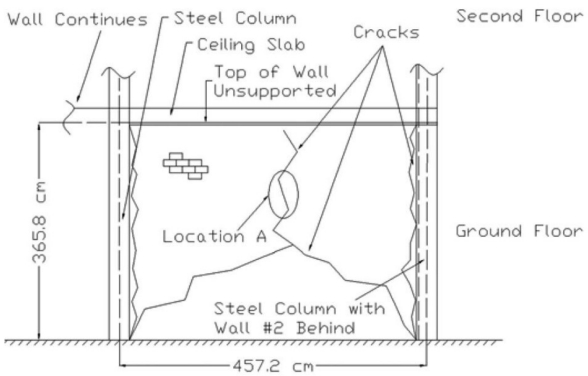

Fig. 13. Pattern of cracks developed on the ground floor partition wall (Wall #1) (Zapata J. B. and Weggel C. D., 2008)

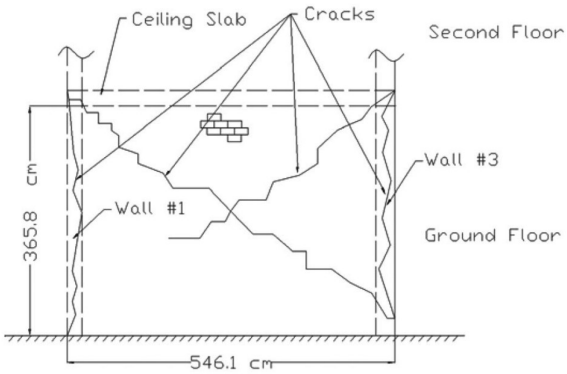

Fig. 14. Pattern of cracks developed on the ground floor load bearing wall (Wall #2) (Zapata J. B. and Weggel C. D., 2008)

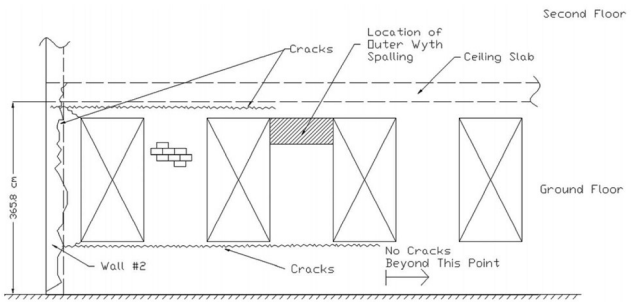

Fig. 15. Pattern of cracks developed on the ground floor load bearing wall (Wall #3) (Zapata J. B. and Weggel C. D., 2008)

230 mm thick walls was found to be much larger than 110 mm (wall thickness). The wall with a thickness of 350 mm experienced much lesser maximum deflection than other walls. The effect of boundary condition and wall thickness on the deflection performance of the URM walls was found to be significant under the applied reflected peak pressures.

2.6 Abou-Zeid M. B. et al. (2011) [2]

The authors performed a series of blast tests to investigate the arching action of 990 mm x 2190 mm x 200 mm URM walls, constructed with two-cell concrete blocks (CMUs) of size 190 mm x 190 mm x 390 mm, subjected to reflected peak pressures generated from the high explosive charges

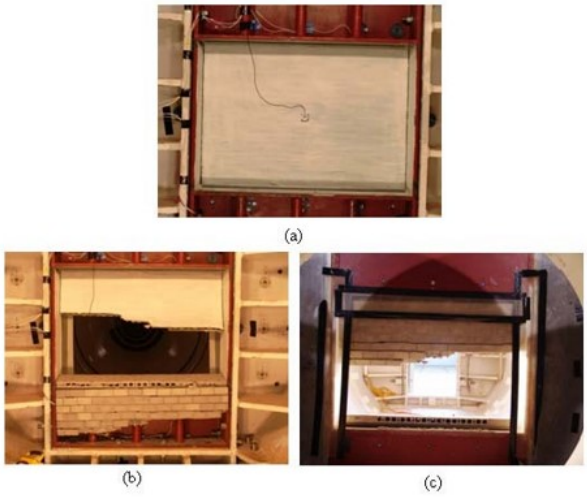

Fig. 16. Damage in Wall #1 (wall with PU coating): (a) Pre-test view, (b) Posttest view (back side), and (c) Post blast test view (front side) (Irshidat M. et al., 2009)

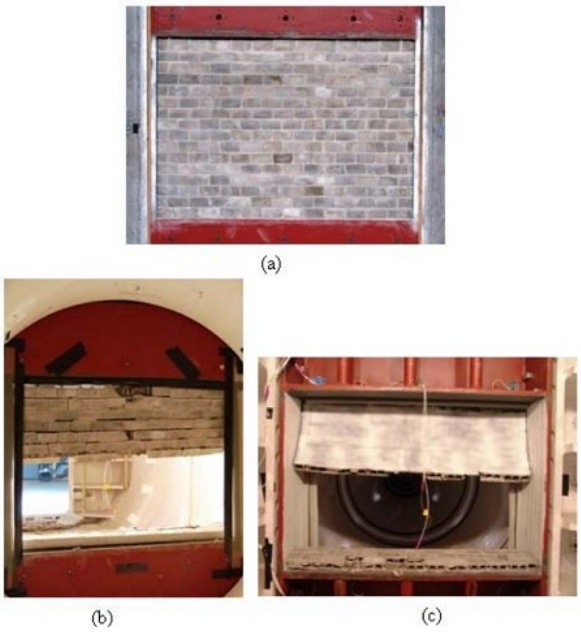

Fig. 17. Damage in Wall #2 (wall with PU-XGnP coating): (a) Pre-test view, (b) Post blast test view (front side), and (c) Post blast test view (back side) (Irshidat M. et al., 2009)

Fig. 18. Damage in Wall #3 (wall with PU-POSS coating): (a) Post blast test view (back side), and (b) Post blast test view (front side) (Irshidat M. et al., 2009)

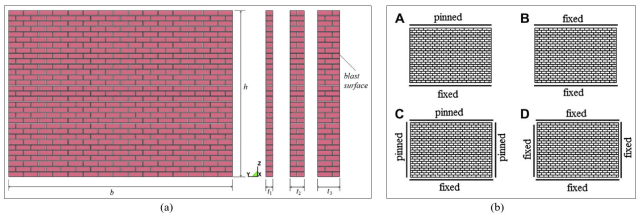

Fig. 19. (a) Wall details and (b) boundary conditions considered by Wei X. and Stewart G. M. (2010) [24]

	$\alpha_t = \alpha_c$	ν	σ_{st0} (MPa)	σ_{sc0}(MPa)	σ_{sttt0} (MPa)	ε_{st0}	ε_{sc0}
Brick1 (B40)	1.0	0.15	2.50	40.00	1.00	0.00024	0.0050
Brick2 (B30)	1.0	0.15	1.88	30.00	0.75	0.00021	0.0043
Brick3 (B20)	1.0	0.15	1.25	20.00	0.50	0.00017	0.0035
Mortar1 (M5)	1.0	0.2	0.83	5.00	0.33	0.00037	0.0022
Mortar2 (M10)	1.0	0.2	1.67	10.00	0.67	0.00052	0.0031
Mortar3 (M15)	1.0	0.2	2.50	15.00	1.00	0.00063	0.0038

Fig. 20. Material properties of brick and mortar (Wei X. and Stewart G. M., 2010)

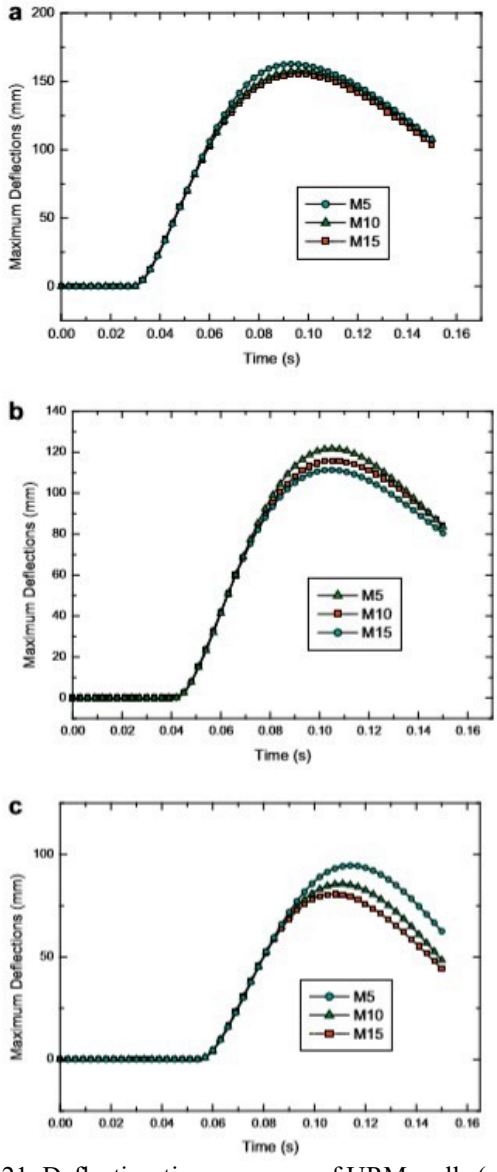

Fig. 21. Deflection-time response of URM walls (of different mortar strength) at different standoff distances obtained by Wei X. and Stewart G. M. (2010) [24]: (a) 20 m, (b) 25 m, and (c) 30 m

(AN/FO) detonated at varying standoff distances (between 3 and 20 m) in the free field. The authors explained the arching action of the one-way URM wall as follows: "After the formation of the tensile cracks at the center and ends of the rigidly supported wall, the wall behaves as two rigid segments, with each segment or part rotating about its end support until either the masonry crushes or the two segments breakthrough". The thickness of the mortar joints was 10 mm. Type-S mortar as per *Canadian Standards Association: Mortar and grout for unit masonry,* CAN/CSA A179-2004 (R2014) [9] was used for the wall construction. The mortar mix proportion, Portland cement: lime: dry sand, was 1.00:0.20:3.50. The average compressive strength of the mortar was 17.90 MPa with a coefficient of variation of 8.70%. The dimensions of each wall were 11 courses high (2190 mm) by 2.50 courses wide (990 mm). The average values of Young's modulus, compressive strength, and tensile strength of concrete blocks were 22.87 GPa, 25.85 MPa, and 0.37 MPa, with a coefficient of variation of 22.56%, 7.06%, and 16.93%, respectively. The walls were divided into three groups: Group-I comprised of five walls (W1-W5) which were designed to study the arching action of the walls under blast loading (see Fig.-24). Group-II comprised of two walls (W6 & W7) which were designed to examine the effect of pre-cracking on the out-of-plane capacity of arching URM concrete walls. Group-III was composed of only one wall (W8) constructed to investigate the debris hazard of the arching wall subjected to close-in blast loading. Two hollow steel sections of size 76.2 mm x 50.8 mm, welded to a structural steel plate, were used to streamline the top and bottom faces of the walls against the steel frame of the container with the objective to restrain the wall's free rotation at its end and enforce arching in the vertical direction. Besides, the backside of the target wall was supported laterally near the bottom and top courses to eliminate the specimen's sliding during its inward movement. Furthermore, two stainless steel clamps were used at the bottom and top of the walls in order to avoid the wall pull-out of the specimen during the suction phase of the blast wave. Moreover, two flange steel columns (W8x48), welded to the bottom and top steel beams, were utilized in order to increase the flexural rigidity of the steel container frame. Steel columns were designed to resist the maximum thrust force of 707.65 kN/m, computed using the empirical equation proposed by Monk B. C. (1958) [18]:

$$T_{max} = \frac{3}{8} f'_m d \left(1 - \frac{d_1}{d}\right) \quad \text{Eq. (1)}$$

Where f'_m = Compressive strength of brick (25.85 MPa); d = thickness of the wall (190 mm); and d_1 = thickness of air space within the URM wall (117 mm). To develop arching action of the wall, the end supports of the wall should be able to withstand maximum thrust force without yielding the supports. Three linear variable differential transformers (LVDTs) with a maximum stroke of 300 mm were installed at the fifth, sixth, and ninth courses of the walls to measure displacements. Results revealed that the arching action significantly improves the blast resistance capacity of the walls by increasing the frictional forces developed between the courses of the masonry.

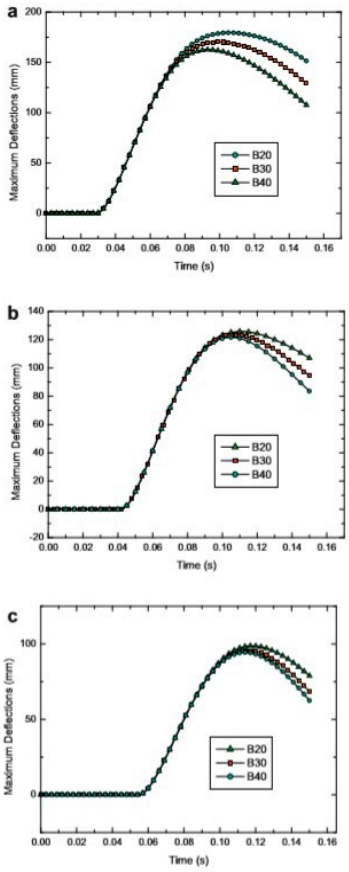

Fig. 22. Deflection-time response of URM walls (of different brick strength) at different standoff distances obtained by Wei X. and Stewart G. M. (2010) [24]: (a) 20 m, (b) 25 m, and (c) 30 m

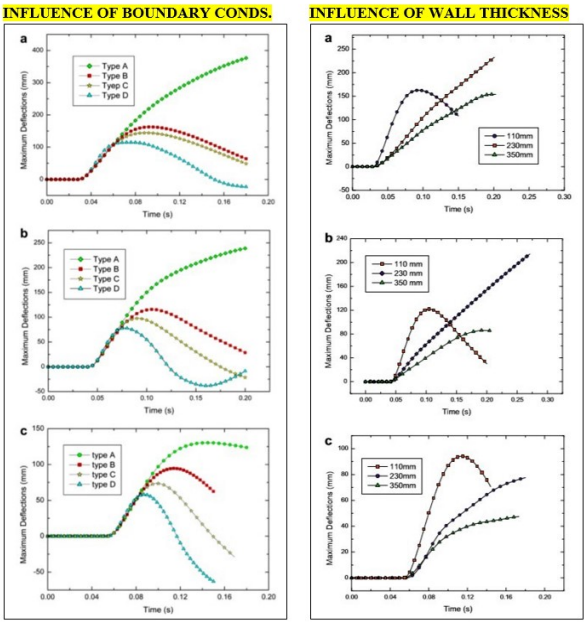

Fig. 23. Deflection-time response of URM walls at different standoff distances obtained by Wei X. and Stewart G. M. (2010) [24]: (a) 20 m, (b) 25 m, and (c) 30 m

Group	Shot #	Specimen #	Charge size ANFO (kg)	Standoff distance (m)
I	1	W1	50	15.0
	2	W2	100	15.0
	3	W3	150	15.0
	4	W4	200	15.0
	5	W5	250	15.0
II	6	W6	15	19.4
	7		25	19.4
	8		50	19.4
	9		75	19.4
	10		153	17.0
	11	W7	30	20.0
	12		100	20.0
	13		250	17.0
III	14	W8	30	3.0

Fig. 24. Test matrix of free field explosion tests conducted by Abou-Zeid M. B. et al. (2011) [2]

2.7 Ahmad S. et al. (2014) [3]

The authors conducted a series of explosion tests on a 2000 mm x 2000 mm x 370 mm free-standing URM wall subjected to blast pressures generated by detonating high explosive charges (Nitro-glycerine dynamite) at varying standoff distances (between 3 and 4 m) in free air, and derived several empirical relations to predict air-blast and ground shock wave parameters such as peak overpressure, the arrival time of air-blast wave, rising time of shock wave, decreasing time, positive phase duration, peak reflected pressure, peak particle acceleration, the arrival time of ground shock, duration of the ground shock wave, and the time lag between air-blast and ground shock waves reaching to the wall. The mass of the explosive charge was varied from 4 to 14 kg with an increment of 2 kg. The wall was constructed with solid clay bricks having a mass density of 1800 kg/m^3, the average compressive strength of 6.76 MPa, Poisson's ratio of 0.17, and Young's modulus of 6.08 GPa. Different measuring devices such as pressure transducers (PCB), strain gauges, tri-axial accelerometers, and high-speed video cameras were used to measure and record the dynamic responses. The results were compared with those predicted by: (1) *Conventional Weapons Effects Program* (CONWEP 2.0) [1, 12]; (2) UFC 3-340-02 (US Department of Defense, 2008) [23]; (3) AASTP-1 (2010) [19]; (4) Brode L. H. (1959) [8] empirical equation; (5) Henrych J. (1979) [13] empirical relationship; (6) Wu C. and Hao H. (2005) [25] empirical equation; (7) Ahmad S. (2012) [4] empirical relationship; and (8) Siddiqui I. J. and Ahmad S. (2007) [22] empirical equation. The measured peak overpressures were found to be in close agreement with those computed from CONWEP 2.0 model and AASTP-1 (2010). The variation among the peak overpressures produced by the empirical equations given by Brode H. L. (1959); Henrych J. (1979); and Ahmad S. (2012) was found to be larger in the scaled distance range, $1.72 \leq Z\ (\text{m/kg}^{1/3}) \leq 2.28$. Fig.-25 shows the variation of measured maximum (tensile) and minimum (compressive) principal stresses with time for charge weights of 4, 6, 8, and 12 kg. They noticed that the walls had completely lost their load carrying capacities as the stresses tend to decrease after the blast (see Fig.-25). Fig.-26 shows the observed crack pattern. It was observed that the crack depth grows with increasing the amount of Nitroglycerin dynamite. Besides, a large horizontal crack had appeared on the front and back faces approximately at mid-height of the wall exposed to a peak overpressure of 0.21 MPa generated from 12 kg Nitro-glycerine dynamite at a standoff distance of 3.50 m (see Fig.-26). Under the explosive load of 14 kg, the wall felled along the weak plane i.e. along the horizontal crack. However, negligible damages and cracks were observed when the wall was exposed to an explosive load of 6 kg. The following are the equations derived using the computed results:

$$P_{OP}\ or\ P_{so} = 3.495 \left(\frac{S}{W^{\frac{1}{3}}}\right)^{-3.408} \quad \text{(MPa)} \qquad \text{Eq. (2)}$$

$$t_A = \frac{8.534}{C_a} \left(\frac{S}{W^{\frac{1}{3}}}\right)^{-0.996} \quad \text{(s)} \qquad \text{Eq. (3)}$$

$$t_1 = 0.0014 \left(\frac{S}{W^{\frac{1}{3}}}\right)^{-0.759} \quad \text{(s)} \qquad \text{Eq. (4)}$$

$$t_2 = 0.0005 \left(\frac{S}{W^{\frac{1}{3}}}\right)^{2.159} \quad \text{(s)} \qquad \text{Eq. (5)}$$

$$t_d = t_1 + t_2 \quad \text{(s)} \qquad \text{Eq. (6)}$$

$$PPA = 42.96 \left(\frac{S}{W^{\frac{1}{3}}}\right)^{-1.774} \quad \text{(g)} \qquad \text{Eq. (7)}$$

$$t_{A2} = \frac{46.17}{C_s} \left(\frac{S}{W^{\frac{1}{3}}}\right)^{-1.32} \quad \text{(s)} \qquad \text{Eq. (8)}$$

$$t_S = 0.1308 \left(\frac{S}{W^{\frac{1}{3}}}\right)^{-1.603} \quad \text{(s)} \qquad \text{Eq. (9)}$$

$$T_{lag} = t_A - t_{A2} \quad \text{(s)} \qquad \text{Eq. (10)}$$

Here, S = Standoff distance (m); W = Explosive charge or amount of TNT (kg); P_{OP} *or* P_{SO} = Peak overpressure or incident blast pressure; C_a = Speed of sound in air (≈340 m/sec); t_A = Arrival time of air-blast wave; t_1 = Rising time; t_2 = Decreasing time; t_d = Positive phase duration; PPA = Peak particle acceleration; t_{A2} = Arrival time of ground shock; C_S = Seismic velocity of soil (≈1524 m/sec); t_S = Duration of ground shock; and T_{lag} = Time lag between air-blast and ground shock waves.

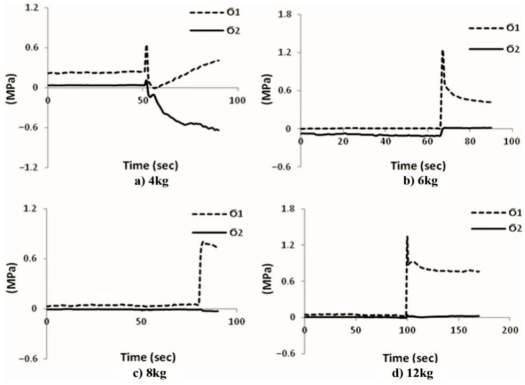

Fig. 25. Variation of principal stresses with time for different charge sizes (Ahmad S. et al., 2014)

(a) 6 kg (b) 12 kg

Fig. 26. Post-test view of URM walls tested for different explosive loads by Ahmad S. et al. (2014) [3]: (a) 6 kg, and (b) 12 kg

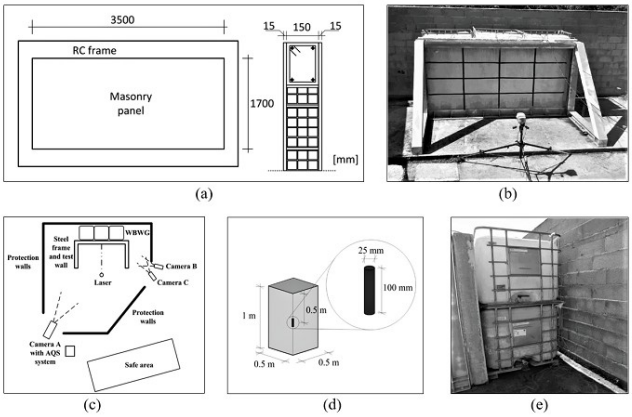

(a) (b) (c) (d) (e)

Fig. 27. Test setup [17]: (a) Description of wall, (b) Supported steel structure and wall, (c) Layout of test setup, (d) Description of explosive charge, and (e) Water containers

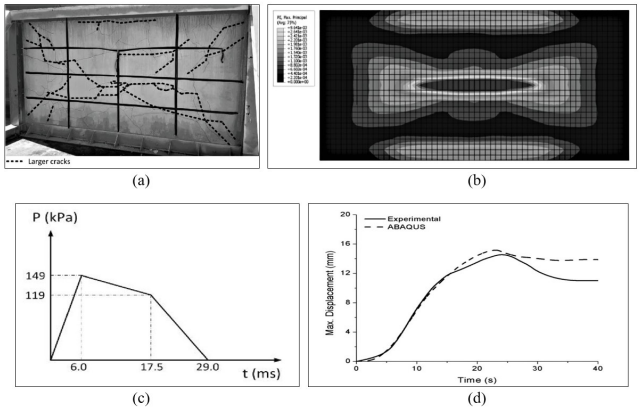

(a) (b) (c) (d)

Fig. 28. Dynamic responses obtained by Joao P. et al. (2014) [17]: (a) Observed crack patterns, (b) Distribution of plastic strain, (c) Blast pressure – time history, and (d) Displacement – time histories

2.8 Joao P. et al. (2014) [17]

The authors experimentally investigated the behavior of 1700 mm x 3500 mm x 180 mm URM wall, constructed with clay bricks, subjected to a reflected peak pressure of 0.149 MPa generated from the cylindrical-shaped explosive charge placed inside a cuboidal shaped metallic container (see Fig.-27). The metallic container was placed inside thick plastic water containers act as underwater blast wave generators (WBWG). WBWGs converted the detonation energy into kinetic energy and allowed a surface area distribution of produced blast pressures. The concept behind the use of WBWGs was to reduce the atmospheric sound waves and to avoid the generation of high-velocity fragments.

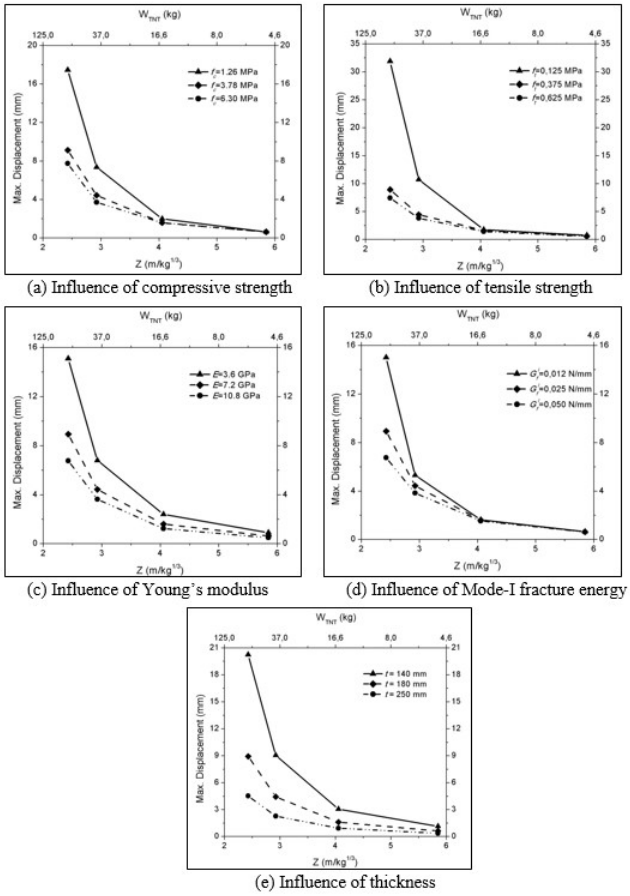

(a) Influence of compressive strength (b) Influence of tensile strength (c) Influence of Young's modulus (d) Influence of Mode-I fracture energy (e) Influence of thickness

Fig. 29. Displacement vs scaled distance responses obtained by Joao P. et al. (2014) [17]

The wall was placed inside a reinforced concrete (RC) frame supported by the steel structure. Sufficient reaction to the wall's RC frame was provided by the steel structure supporting the structural element i.e. reinforced concrete frame. Besides, large water containers (one cubic meter) were placed on one side of the wall to act as underwater blast wave generators and to apply the desired impulsive load on the surface of the wall. On the other side of the wall, various measuring devices were installed to record the responses and capture the dynamic behavior. Large cracks were mostly concentrated at the mid-height of the wall and extended to the top and bottom edges as well as corners of the wall (Fig.-28(a)). The results were compared and found to be in good agreement with the predictions of the concrete damaged plasticity (CDP) model available in the ABAQUS/CAE program (Fig.-28(d)). Parametric investigations were also conducted to study the effect of compressive strength, tensile strength, young's modulus of masonry, Mode-I fracture energy, and wall thickness on the tested URM wall. Fig.-28(b) shows the distribution of plastic strain obtained from the CDP model. The pattern of the plastic strain was found similar to the crack pattern observed by Joao P. et al. (2014) after the blast test. It was concluded that the influence of Young's modulus on the blast response of the tested walls was more effective in comparison to other influences considered.

Table-1. Summary of the URM walls subjected to explosive-induced blast loading: Part I

No.	Research information			
	Research team	Year published	Masonry type	Supporting structure type
1	Carney P. and Myers J. J.	2005	Concrete blocks (CMUs)	RC frame
2	Hrynyk D. T. and Myers J. J.	2008	Clay bricks; Concrete blocks; Wood-fiber fly ash bricks	RC and Steel frame structure
3	Zapata J. B. and Weggel C. D.	2008	Not specified	RC and Steel frame structure
4	Irshidat M. et al.	2009	Concrete blocks	Steel frame
5	Wei X. and Stewart G. M.	2010	Clay bricks	-
6	Abou-Zeid M. B. et al.	2011	Two-cell concrete blocks	Steel frame
7	Ahmad S. et al.	2014	Clay bricks	-
8	Joao P. et al.	2014	Clay bricks	RC and Steel frame structure

Table-2. Summary of the URM walls subjected to explosive-induced blast loading: Part II

No.	Research information			Strengthening technique adopted
	Wall thickness (mm)	Average compressive strength of the masonry (MPa)	Explosive used	
1	101.60	Not specified	Pentolite	GFRP strips; GFRP rods
2	102.00	10.30; 9.00; 6.90	Airbag system	Polyurea coating; GFRP grid with polyurea
3	300; 200	13.10	Not specified	-
4	115	-	Blast wave simulator	Polyurea coating; Polyurea with exfoliated graphene nanoplatelets (PU-XGnP); Polyurea with polyhedral oligomeric silsesquioxane (PU-POSS);
5	110; 230; 350	12.24	TNT	-
6	200	25.85	AN/FO	-
7	370	6.76	Nitro-glycerine dynamite	-
8	180	3.78 (Dynamic); 1.24 (Static)	Pentaerythritol tetranitrate	-

Table-3. Summary of the URM walls subjected to explosive-induced blast loading: Part III

No.	Experimental results verified	Software employed	Type of response used	Damage categories
1	Yes	SDOF method	Damage; Blast pressures	Light damage; Heavy damage; Failure
2	No	-	Failure modes; Cracks; Deflection performance; Load-carrying capacity	Instability failure; Flexural failure; Anchorage failure of Polyurea near supports
3	Yes	SDOF method	Blast pressure; Damage; Displacement; Damage state of load-bearing wall relative to its collapse limit state	-
4	No	-	Mid-span deflection; Damage; Blast pressure	-
5	No	-	Deflection performance	-
6	No	-	Blast resistance capacity; Arching action	-
7	Yes	ConWEP 2.0 Model	Peak overpressures; Time of arrival of blast wave; Peak particle acceleration; Time lag; Arrival time of ground shock; Stresses	-
8	Yes	ABAQUS/CAE	Blast pressures; Cracks; Displacement	-

Summary

This investigation sought to better understand the influence of brick strength, mortar strength, wall thickness, Young's modulus of masonry, and boundary conditions on the performance of the clay brick and concrete block unreinforced masonry walls under blast loading. Also, the effects of Polyurea (PU) coating, PU with exfoliated graphene nanoplatelets (PU-XGnP), PU with polyhedral oligomeric silsesquioxane (PU-POSS), and glass fiber reinforced polymer (GFRP) composites on the damage resistance of the walls have been discussed. Despite the review of eight experimental studies, this is still a nascent area of research. As such, prior to further development, it is necessary to cross-correlate them. The review of the available experimental studies on the blast response of the

URM walls is summarized in the following three tables (Tables 1to3).

Based on a closer review of the reported experimental investigations, the authors feel that the following aspects should and could be considered for subsequent research:

1. High-fidelity FE models should be developed in order to accurately simulate the response of the URM walls under blast loading.
2. Variation of stresses developed in the material of the wall should be described.
3. Geometric parameters of cracks and estimation of damage dissipation energy should be accounted for both experimental and numerical investigations.
4. The effect of explosive-induced ground shock on the performance of the URM walls has not been investigated and should be examined.
5. The polymer materials used so far to improve the damage resistance of the walls require protective clothing and expensive. Therefore, more innovative materials should be developed to overcome such issues without sacrificing mechanical performance.
6. Hybrid wall systems should be developed to improve the blast resistance of the wall.
7. Design guidelines and tools should be developed for the retrofit methodology to resist explosive-induced blasts.

Acknowledgement

The authors are grateful for helpful discussions with Professor T K Datta of the Department of Civil Engineering of Indian Institute of Technology Delhi (New Delhi, India-110 016).

Disclosures

Free Access to this article is sponsored by SARL ALPHA CRISTO INDUSTRIAL.

References

1. ABAQUS/CAE FEA program 2017. Concrete damaged plasticity model. ABAQUS DS-SIMULIA User Assistance Manual, 2017.
2. Abou-Zeid M B, El-Dakhakhni W W, Razaqpur G A, and Foo S. Response of arching unreinforced concrete masonry walls to blast loading. Journal of Structural Engineering, ASCE, 2011; 137(10): 1205-1214.
3. Ahmad S, Elahi A, Pervaiz H, Rahman A G A, and Barbhuiya S. Experimental study of masonry wall exposed to blast loading. Materials De Construction, 2014; 64(313): 1-11.
4. Ahmad S, Taseer M, and Pervaiz H. Effects of impulsive loading on reinforced concrete structures. Technical Journal, University of Engineering and Technology, Pakistan, 2012.
5. American Society for Testing and Materials. Standard test method for compressive strength of hydraulic cement mortars (using portions of prisms broken in flexure). Design Standard, ASTM C349-18(2005).
6. Anas M S, Ansari I Md, and Alam M. A study on existing masonry heritage building to explosive-induced blast loading and its response. International Journal of Structural Engineering, 2020.
7. Anas M S, Ansari I Md, and Alam M. Performance of masonry heritage building under air-blast pressure without and with ground shock. Australian Journal of Structural Engineering, Taylor & Francis, 2020; DOI: 10.1080/13287982.2020.1842581.
8. Brode L H. Blast wave from a spherical charge. The Physics of Fluids, 1959; 2(217).
9. Canadian Standards Association. Mortar and grout for unit masonry. Design Manual, CAN/CSA A179-2004 (R2014), 2014.
10. Carney P and Myers J J. Out-of-plane static and blast resistance of unreinforced masonry wall connections strengthened with FRP. American Concrete Institute Special Publication, ACI, 2005; 230(14).
11. Edri E I, Yankelevsky Z D, Rabinovitch O. Blast response of one-way arching masonry walls. International Journal of Impact Engineering, 2020; 141: 1-16.
12. Goel D M and Matsagar A V. Blast-resistant design of structures. Practice Periodical on Structural Design and Construction, 2014, ASCE, 19(2): 04014007-1-9.
13. Henrych J. The dynamics of explosion and its use. Elsevier, Scientific Publishing Company, Amsterdam, 1979; 8(3): 1-562.
14. Hrynyk D T and Myers J J. Out-of-plane behavior of URM arching walls with modern blast retrofits: experimental results and analytical model. Journal of Structural Engineering, ASCE, 2008; 134(10): 1589-1597.
15. Irshidat M, Al-Ostaz A, Cheng A, and Mullen C. Blast resistance of unreinforced masonry (URM) walls retrofitted with Nano Reinforced elastomeric materials. Structures Congress 2009, Texas, US, 2009: 2133-2142.
16. Jayasinghe C. Characteristics of different masonry units manufactured with stabilized earth. International Symposium on Earthen Structures, Indian Institute of Science, Bangalore, 2007; 22-24: 252-258.
17. Joao P, Jose C, and Paulo B L. Experimental study on masonry infill walls under blast loading. 9th International Masonry Conference, Guimaraes, 2014; 1-11.
18. Monk B C. Resistance of structural clay masonry to dynamic forces. Research Report, Geneva, 1958; (7).
19. North Atlantic Treaty Organization. Manual of Nano safety guidelines for the storage of military ammunition and explosives. Technical Manual, NATO-AASTP-1(2010).
20. Pereira M J, Campos J, and Lourenco B P. Masonry infill walls under blast loading using confined underwater blast wave generators (WBWG). Engineering Structures, 2015; 92(1), 69-83.
21. Remennikov M A. A review of methods for predicting bomb blast effects on buildings. Journal of Battlefield Technology, 2(3): 5-10.
22. Siddiqui I J and Ahmad S. Impulsive loading on a concrete structure. Proceedings of the Institution of Civil Engineers, Structures & Buildings, 2007; 160(4): 231-241.

23. U S Army Corporations of Engineers. Structures to resist the effects of accidental explosions. Design Manual, Unified Facilities Criteria, UFC (3-340-02), 2008.

24. Wei X and Stewart G M. Model validation and parametric study on the blast response of unreinforced masonry walls. International Journal of Impact Engineering, 2009; 37(11): 1150-1159.

25. Wu C and Hao H. Modeling of simultaneous ground shock and airblast pressure on nearby structures from surface explosions. International Journal of Impact Engineering, 2005; 31(6): 699-717.

26. Zapata J B and Weggel C D. Collapse study of an unreinforced masonry bearing wall building subjected to internal blast loading. Journal of Performance of Constructed Facilities, ASCE, 2008; 22(2): 92-100.

27. Zhuge Y. FRP-retrofitted URM walls under in-plane shear: review and assessment of available models. Journal of Composites for Construction, ASCE, 2010; 14(6): 743-753.